Eur. Phys. J. C (2011) 71: 1511
DOI 10.1140/epjc/s10052-010-1511-3

THE EUROPEAN PHYSICAL JOURNAL C

Regular Article - Experimental Physics

A fresh look at $\eta_2(1645)$, $\eta_2(1870)$, $\eta_2(2030)$ and $f_2(1910)$ in $\bar{p}p \to \eta\pi^0\pi^0\pi^0$

A.V. Anisovich[3], **C.J. Batty**[2], **D.V. Bugg**[1,a], **V.A. Nikonov**[3], **A.V. Sarantsev**[3]

[1] Queen Mary, University of London, London E1 4NS, UK
[2] Rutherford Appleton Laboratory, Chilton, Didcot, OX11 OQX, UK
[3] St. Petersburg Nuclear Physics Institute, Gatchina, St. Petersburg district 188350, Russia

Received: 9 September 2010 / Revised: 3 November 2010 / Published online: 12 January 2011
© The Author(s) 2010. This article is published with open access at Springerlink.com

Abstract There is a large discrepancy between results of Crystal Barrel and WA102 for the branching ratio $R = BR[\eta_2(1870) \to a_2(1320)\pi]/BR[\eta_2(1870) \to f_2(1270)\eta]$. An extensive re-analysis of the Crystal Barrel data redetermines branching ratios for decays of $\eta_2(1870)$, $\eta_2(1645)$, $\eta_2(2030)$ and $f_2(1910)$. This re-analysis confirms a small value for R of 1.60 ± 0.39, inconsistent with the value 20.4 ± 6.6 of WA102. The likely origin of the discrepancy is that the WA102 data contain a strong $f_2(1910) \to a_2\pi$ signal as well as $\eta_2(1870)$. There is strong evidence that the $\eta_2(1870)$ has resonant phase variation. A peak in $f_2(1270)a_0(980)$ confirms closely the parameters of the $a_2(2255)$ resonance observed previously. A peak in $\eta_2(2030)\pi$ is interpreted naturally in terms of $\pi_2(2245)$ with reduced errors for mass and width $M = 2285 \pm 20(stat) \pm 25(syst)$ MeV, $\Gamma = 250 \pm 20(stat) \pm 25(syst)$ MeV.

1 Introduction

The objective of this paper is to re-examine data from Crystal Barrel (CBAR) [1–3] concerning $\eta_2(1645)$, $\eta_2(1870)$, $\eta_2(2030)$ and $f_2(1910)$. One motivation is to study a large discrepancy for branching ratios of $\eta_2(1870)$. Earlier CBAR work found a branching ratio

$$R = \frac{BR[\eta_2(1870) \to a_2(1320)\pi]}{BR[\eta_2(1870) \to f_2(1270)\eta]} = 1.27 \pm 0.17, \qquad (1)$$

see Table 5 of Ref. [3]. This is much smaller than the value 20.4 ± 6.6 claimed by the WA102 collaboration in central production of $\eta\pi\pi$ [4]. Other branching ratios determined by the CBAR data are redetermined here. This re-analysis incorporates many further details of spectroscopy in this mass range which have appeared since the year 2000.

A review of these earlier publications will set the scene and introduce the relevant resonances. For a comprehensive review of the CBAR work with $\bar{p}$ in flight see Ref. [5]. The first study of $\eta_2(1645)$ and $\eta_2(1870)$ in CBAR data was at two beam momenta: 1200 and 1940 MeV/c [1, 2]. The $\eta_2(1645)$ was observed decaying to $a_2(1320)\pi$ and $a_0(980)\pi$. No other a_0 or a_2 appear in the data, so a_0 will be used hereafter as a shorthand for $a_0(980)$ and likewise a_2 for $a_2(1320)$.

There was also a strong $f_2(1270)\eta$ signal near its threshold ∼1810 MeV. It could not be explained as the high mass tail of $\eta_2(1645)$. The reason was that a single $\eta_2(1645)$ decaying to $f_2\eta$ would contain a large $f_2\eta$ signal in both numerator and denominator of the Breit-Wigner amplitude; cancellation between numerator and denominator cannot accommodate the large $f_2(1270)\eta$ signal. The data were fitted with the addition of the $\eta_2(1870)$ though the data did not rule out the possibility of a non-resonance threshold effect at that time.

The majority of CBAR data with $\bar{p}$ in flight were taken in 1996. For $\eta 3\pi^0$, statistics were a factor 7 higher than earlier data at each of nine beam momenta ranging from 600 to 1940 MeV/c, i.e. an overall increase of statistics by a factor ∼30. There are typically 25–30 K events at each beam momentum and a total of 213 K events.

Figure 1 shows scatter plots from CBAR data in three ranges of $\eta\pi\pi$ mass. Figure 1(a) shows the $\eta_2(1645)$ mass range; there is a vertical band due to $a_2\pi$ and also a peak in $\pi\pi$ near 1 GeV. The spin analysis ruled out $f_0(980)$, showing that the peak in $\pi\pi$ is due to the low mass tail of $\eta_2(1870) \to f_2(1270)\eta$. Figure 1(b) shows the $\eta_2(1870)$ mass range. The $a_2(1320)$ and $f_2(1270)$ bands appear of similar strength; however, the f_2 is somewhat broader and therefore stronger. There is clearly no large excess of a_2 decays in this mass interval. The branching ratio quoted by WA102 would require an $\eta_2(1870) \to a_2\pi$ signal a fac-

[a] e-mail: david.bugg@stfc.ac.uk

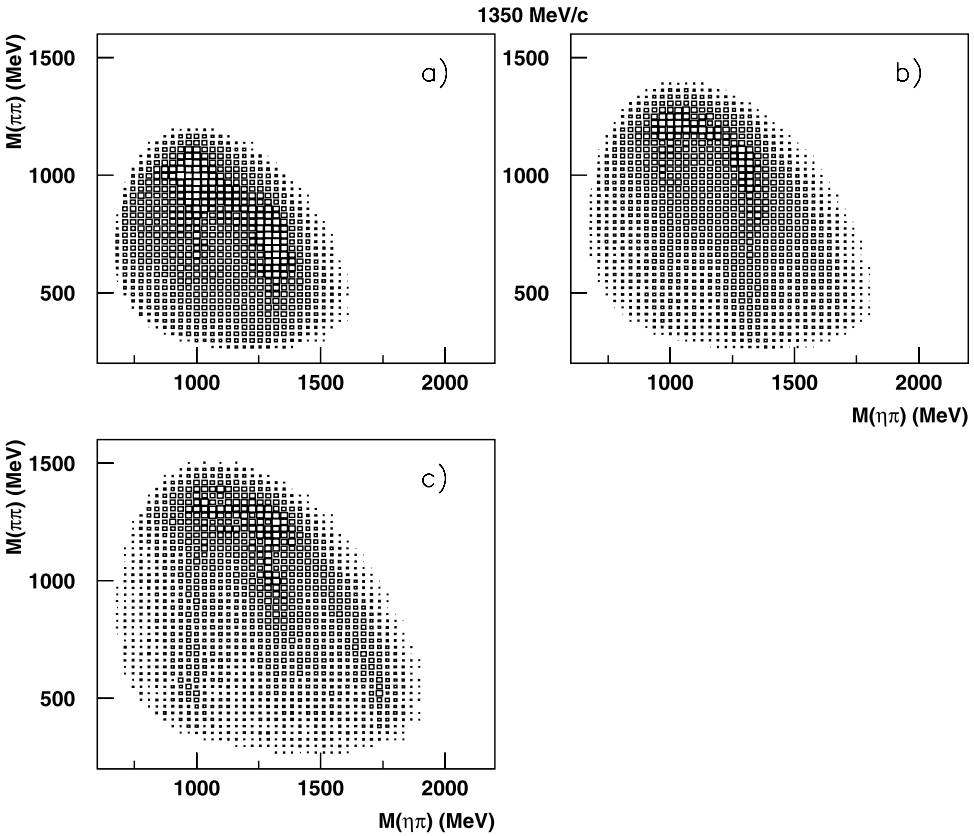

Fig. 1 Scatter plots of $M(\pi\pi)$ vs. $M(\eta\pi)$ for three ranges of $M(\eta\pi\pi)$: (**a**) 1560–1750 MeV, centred on $\eta_2(1645)$, (**b**) 1775–1945 MeV over $\eta_2(1870)$ and (**c**) 1945–2115 MeV, centred on $\eta_2(2030)$. The beam momentum is 1350 MeV/c

tor ~ 3.5 larger than $f_2(1270)\eta$ when one allows for relative decay rates of $a_2 \to \eta\pi$ and $f_2(1270) \to \pi^0\pi^0$ and for charge combinations. Figure 1(c) shows the mass range of $\eta_2(2030)$; there is a peak where $a_2(1320)$ and $f_2(1270)$ bands cross. The $a_2\pi$ band is strong and $f_2(1270)\eta$ is weaker. Note also that weak $a_0(980)$ bands are visible in all three panels.

There is additional evidence for $\eta_2(2030) \to f_2(1270)\eta$ and $a_2\pi$ in further CBAR data for $\bar{p}p \to \eta\pi^0\pi^0$, see Fig. 11 of Ref. [6]. A distinctive feature of this state is its strong decay to $[a_2\pi]_{L=2}$, where L is the orbital angular momentum in the decay.

Following the year 2000 publication of $\eta 3\pi^0$ results, a combined analysis was made of 10 sets of data with isospin $I = 0$ and C-parity $+1$. Six of these were CBAR data for $\bar{p}p$ in flight $\to \pi^0\pi^0$, $\eta\eta$, $\eta\eta'$, $\eta\pi^0\pi^0$, $\eta'\pi^0\pi^0$ and $\eta\eta\eta$ [7]. The other four were high quality differential cross sections and polarisations for $\bar{p}p \to \pi^+\pi^-$ from two experiments: Eisenhandler et al. [8] and PS172, Hasan et al. [9]. This analysis revealed two towers of resonances centred at ~ 2000 and 2270 MeV, with all J^P for $q\bar{q}$ states expected in this mass range. Most have been observed in at least three sets of data. Polarisation data provide a clean separation of $\bar{p}p$ ${}^3P_2$ and ${}^3F_2$ states. The $f_2(1910)$ of the PDG [10] was confirmed and identified as dominantly ${}^3P_2$; a neighbouring ${}^3F_2$ state was observed at 2001 MeV. Further $f_2(2240)$ ${}^3P_2$ and $f_2(2295)$ ${}^3F_2$ states were also observed. In the new analysis reported here, the first three of these f_2 states play a significant role. The $f_2(1910)$ lies close to $\eta_2(1870)$ and is important for the discussion of WA102 data.

In 2001, a combined analysis was also made of data on $I = 1$, $C = +1$ states [11]. The spectrum of states is less complete than for $I = 0$, $C = +1$, because of the lack of polarisation data. Nonetheless, an $a_2(2255)$ appeared clearly in three channels of data. Secondly, there is a less well identified $\pi_2(2245)$. These two states now appear in the analysis reported here. So, in summary, the picture has developed significantly since the earlier analysis of $\eta 3\pi^0$.

The $\eta 3\pi^0$ channel may appear to be a complicated channel to analyse, because of the multiplicity of $\eta\pi^0$ and $\pi^0\pi^0$ combinations. However, $\eta_2(1645)$ and $\eta_2(1870)$ were found here; also, once one knows the mass and width of $\eta_2(2030)$ from $\eta\pi\pi$ final states, it is easily detected in the present data via its strong decay to $[a_2\pi]_{L=2}$, which has a very distinctive angular dependence. Interferences between channels provide intricate information on identifiable resonances, even though the angular correlations cannot be displayed because they are multi-dimensional. It is necessary to work from log likelihood and mass projections of $\eta\pi$, $\pi\pi$, 3π and $\eta\pi\pi$. A valuable check on the analysis is to introduce deliberate errors into angular dependence of amplitudes; genuine signals then drop to low values.

Two alternative starting points have been adopted. The first is the year 2000 analysis, which now improves. The second starts from the WA102 ratio for $\eta_2(1870) \to a_2\pi$ and $f_2(1270)\eta$. This gives a considerably worse fit. After iterations, the two fits converge to a single solution except for minor points of ambiguity in $a_0\pi$ decays. No significantly different solutions have been found at any beam momentum despite searches from a variety of initial parameters.

The layout of the paper is as follows. Sections 2 and 3 go through technical details of the analysis procedure. It may be useful to glance first at figures of later sections, so as to appreciate the rationale for the steps discussed in Sects. 2 and 3; the techniques need to be adapted to what is found in the data. Section 2 introduces the channels which are required and deals with formulae. These are well known from earlier literature, but need to be documented. The one point requiring special treatment is the opening of the $f_2(1270)\eta$ threshold, close to $\eta_2(1870)$. It is necessary to fold the width of $f_2(1270)$ into the phase space for the $f_2\eta$ final state appearing in the Breit-Wigner amplitude. Secondly, the way the spin dependence is treated in terms of partial waves is discussed.

Section 3 presents features of the data. Figure 4 shows mass spectra for 3π, $\pi\pi\eta$, $\pi\eta$ and $\pi\pi$ at one representative momentum, 1642 MeV/c; other momenta show similar features and Fig. 1 of Ref. [3] presents spectra at 1800 MeV/c. This section gives more detailed comparisons with data in further figures.

Section 4 then presents essential results. Table 1 shows changes of log likelihood when each channel is dropped from the fit and all others are re-optimised. This table identifies directly the important channels and their significance levels, and how they vary with beam momentum. Figure 7 presents the cross sections for all reactions as a function of beam momentum; these lead to considerable insight into the physics. Peaks shown in Fig. 8 may be identified with $a_2(2255)$ and $\pi_2(2245)$.

A revised set of branching ratios is derived for $\eta_2(1645)$, $\eta_2(1870)$, $\eta_2(2030)$ and $f_2(1910)$. The strong decay modes change little, but there are some significant changes from the earlier publication in weak channels, for reasons which are understood. The important ratio for $\eta_2(1870) \to a_2(1320)\pi$ and $f_2(1270)\eta$ changes only slightly and remains completely inconsistent with the WA102 result.

Section 5 therefore re-examines WA102 mass projections for $\eta_2(1645)$ and $\eta_2(1870) \to a_0\pi$, $a_2\pi$ and $f_2(1270)\eta$. There is good agreement with CBAR data for $\eta_2(1645) \to a_2\pi$ and $a_0\pi$ and their ratio of intensities. There is also reasonable agreement for the line-shape of $\eta_2(1870) \to f_2(1270)\eta$. So masses and widths of these states agree well between the two experiments. The evidence for the controversial $f_2(1870) \to a_2\pi$ signal rests on a small bump in the $a_2\pi$ mass spectrum in WA102 data. It now appears likely that some or all of this bump is instead due to $f_2(1910)$. This state has a strong decay to $a_2\pi$ and weaker decay to $f_2(1270)\eta$. An earlier WA102 publication in fact claimed to observe $J^P = 2^+$ peaks near 1900 MeV in central production of $a_2(1320)\pi \to \rho\pi\pi$ and in $f_2(1270)\pi\pi$ [12]. Section 6 presents evidence that $\eta_2(1870)$ has resonant phase variation. Section 7 summarises results and draws conclusions.

2 Methodology and formulae for fitting data

The data are fitted by the maximum likelihood method, i.e. fitting every individual event without binning. Log likelihood is normalised so that a change of 0.5 corresponds to a change in χ^2 of 1. For the high statistics available here, log likelihood follows the χ^2 distribution closely as the number of variables is varied. The following channels are fitted:

$$\bar{p}p \to f_2(1270)a_0(980) \tag{2}$$
$$\to a_2(1320)\sigma \tag{3}$$
$$\to \pi_2(1670)\eta \tag{4}$$
$$\to f_1(1285)\pi \tag{5}$$
$$\to \eta(1440)\pi \tag{6}$$
$$\to \eta_2(1645)\pi \tag{7}$$
$$\to \eta_2(1870)\pi \tag{8}$$
$$\to \eta_2(2030)\pi \tag{9}$$
$$\to f_2(1910)\pi \tag{10}$$
$$\to f_2(2001)\pi \tag{11}$$
$$\to f_2(2240)\pi. \tag{12}$$

Here σ stands for the $\pi\pi$ S-wave amplitude. An incoherent phase space background is also included. It arises from experimental cross-talk between the $\eta 3\pi^0$ final state and other final states, e.g. $4\pi^0$ and $\eta\eta\pi^0\pi^0$. This background is known accurately and is discussed in the earlier publication [3]; it is in the range 7.7–9.6%, increasing slowly with beam momentum.

We can dispose of channels (5) and (6) quickly. Their $\pi\pi\eta$ peaks are narrow and have no significant impact on other channels. The $f_1(1285)$ is fitted as decaying purely to $a_0\pi$. Its mass and width need tuning by a few MeV to fit the height and width of the observed peak. The $\eta(1440)$ is fitted with decays to $a_0\pi$ and $\eta\sigma$, with interference between them. There is also evidence for $\eta(1440) \to f_0(980)\eta$, discussed in Ref. [13] and confirmed in [14]. The $\eta(1440)$ appears clearly only at low beam momenta up to 1200 MeV/c and the fit to it does not change significantly from that reported earlier.

Tests have been made for additional resonances produced in $\bar{p}p \to X + \pi$ where X has quantum numbers $J^P = 0^-$, 1^+, 3^+ or 4^+. There is no significant evidence for any of these. The high spin states would be easily detectable from their strong angular dependence. Adding $0^- \to a_0\pi$ and $f_0(980)\eta$ does give a small improvement in log likelihood, typically 20, but this is because these amplitudes have no angular dependence and are prone to picking up noise; there is no discernable optimum in log likelihood as $\pi\pi\eta$ mass is varied. The final fit omits 0^- states other than $\eta(1440)$.

2.1 Treatment of partial waves

Most channels involve a two-stage process $\bar{p}p \to X + \pi$, $X \to Y + \pi$. The orbital angular momentum in the decay to $X + \pi$ will be denoted by ℓ and that in the subsequent decay to $Y + \pi$ by L. The $\bar{p}p$ initial state is a mixture of spin singlet and triplet partial waves. The total spin S is limited to $S_z = \pm 1$ or 0 along the beam direction; $S_z = \pm 1$ give identical angular distributions. A problem in the analysis is the absence of polarisation data. The consequence is that triplet contributions to X are not cleanly separated between $J = \ell$, $\ell \pm 1$ and $\ell \pm 2$. It is therefore not possible to do a full partial wave analysis of both production and decay. This would become possible if data were available at a future date from a polarised target.

Figure 2 sketches the process of production and decay. The a_2 and recoil pion are drawn in the $\bar{p}p$ rest frame. The decay of the a_2 is shown after a Lorentz transformation to the a_2 rest frame. One way of writing amplitudes is to use rotation matrices to express the initial state $|J, J_z\rangle$ in terms of a linear combination quantised along the a_2 direction. This combination is invariant under a Lorentz boost to the rest frame of the a_2 [15]. Then the a_2 decay amplitude may be expressed in terms of the usual Legendre polynomials. The problem with this approach is that the rotation matrices at the first step depend on J.

This problem may be avoided by a procedure known as the Wick rotation. After a Lorentz boost to the rest frame of the a_2, a rotation of axes is made through an angle $-\theta$, the same as in the production process but with opposite sign. Rotation matrices then cancel between the first and second steps. The Wick rotation alters the angles of π and η in the $\bar{p}p$ rest frame, because of the Lorentz boost. It preserves the fact that the initial state is restricted to $J_z = 0$ or 1. Since J is not known, it is however necessary to discard the angular dependence of the production process or parametrise it empirically. The way the programme is written, the Wick rotation is made for every channel and every event just once, and the required amplitudes are stored. This speeds up the analysis by a large factor.

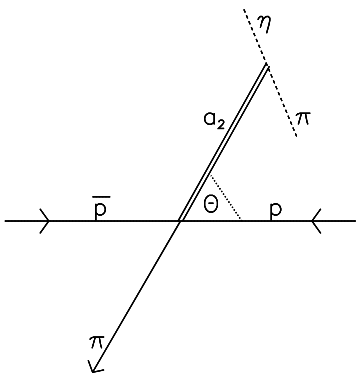

Fig. 2 A sketch of $\bar{p}p \to a_2(1320) \to \eta\pi$

Two improvements of details over the earlier analysis are introduced. For singlet states, $S_z = 0$. The processes $\bar{p}p \to X + \pi$ may go via emission of a pion with orbital angular momentum $\ell \geq 1$, because of the pseudoscalar nature of the pion. For low momenta of the spectator pion, several channels rise steeply, see Figs. 7 and 8 below. This is consistent with P-state production. If the $\eta_2\pi$ final states in reactions (7)–(9) are produced via P-state pion emission, the initial state is restricted to $J^{PC} = 2^{-+}$ unless it is exotic ($J^{PC} = 3^{-+}$ or 1^{-+}). It would be surprising if exotics couple to $\bar{p}p$ and there is no evidence for such exotics in other CBAR data in flight. This leads to the useful restriction that the initial state is spin singlet, with $S_z = 0$. A further point is that $\bar{p}p \to J^{PC} = 2^{-+} \to [2^{-+} + \pi]_{L=1}$ has Clebsch-Gordan coefficients such that the final state is purely $|J' = 2, J'_z = \pm 1, L = 1, L_z = \mp 1\rangle$, where J' is the spin of the η_2. This leads to a distinctive angular dependence for the whole amplitude describing both production and decay. It is helpful in isolating the process $\bar{p}p \to \pi_1(2245) \to [\eta_2(2030)\pi]_{L=1}$. However, in addition we detect some significant production from initial spin triplet states, particularly $\bar{p}p\ J^{PC} = 2^{++} \to [2^{-+} + \pi]_{L=0}$.

Interferences between all channels are included. However, several spin triplet states produced from $\bar{p}p$ may feed a single final state such as $[f_2\pi]_{L=1}$. As a result, interferences between channels are not fully coherent. To accommodate this detail, each interference term is multiplied by a coherence factor which is allowed to optimise in the range ± 2. There are also interferences between two $a_2\pi$ and two $a_0\pi$ combinations for each resonance in $\eta\pi\pi$. These interferences are fully coherent for a single resonance.

2.2 The treatment of phase space

The $\eta_2(1870)$ lies close the $f_2(1270)\eta$ threshold. The intensity of the $f_2\eta$ decay needs to be parametrised so as to include the line-shape of the f_2 into the available phase space. The formula for the general case $\bar{p}p \to X + Z$, where X and Z both have significant width, is given by Eq. (40) in Ref. [16]. This formula is used for channels (2)

and (3), $\bar{p}p \to f_2(1270)a_0$ and $a_2\sigma$. For the simpler case of $\eta_2(1870) \to f_2(1270)\eta$, it reduces to

$$\rho(f_2\eta, s) = \int_{4m_\pi^2}^{(\sqrt{s}-m_\eta)^2} \frac{ds_1}{\pi} \frac{4|p|}{\sqrt{s}\sqrt{s_1}} \times \frac{M\Gamma(s_1)}{(M^2 - s_1)^2 + (M\Gamma(s_1))^2} FF(s), \quad (13)$$

where p is the momentum of the η in the $f_2\eta$ rest frame; $\sqrt{s}$ and $\sqrt{s_1}$ are the corresponding masses of $f_2\eta$ and f_2. Also $FF(s)$ is a form factor for $\eta_2(1870) \to f_2(1270)\eta$. It is taken as a Gaussian $\exp(-\alpha p^2)$, where $\alpha = 4.5$ (GeV/c)$^{-2}$, corresponding to a radius of interaction 0.73 fm for the overlap of f_2 and η. From a wide range of CBAR and other data, α is known with an error of ± 1.0 (GeV/c)$^{-2}$. In the range of the present data, results vary little over the range $\alpha = 3.5 - 5.5$ (GeV/c)$^{-2}$. However, the exponential dependence may be an approximation.

Figure 3 shows $f_2\eta$ phase space v. mass. It peaks at 1.96 ± 0.03 GeV, and rises through half-height at 1.80 GeV. It is desirable to include this s-dependence into the line-shape of $\eta_2(1870)$ at least approximately. This is done by approximating the phase space of $f_2\eta$ by a Fermi function shown by the dashed curve of Fig. 3:

$$F(s) \propto 1.0/\big(1.0 + 1.4\exp\big(5.11\big(1.76^2 - s\big)\big)\big). \quad (14)$$

Then the Breit-Wigner amplitude for $\eta_2(1870) \to f_2\eta$ is

$$f \propto \frac{\rho(f_2\eta, s)}{M^2 - s - iM[\Gamma_1 + \Gamma_2 F(s)]}, \quad (15)$$

where Γ_1 and Γ_2 are constants describing decays to (1) $a_2\pi$ and $a_0\pi$, (2) $f_2\eta$. Above 1.96 GeV, the Fermi function may be an approximation, but the line-shape of $\eta_2(1870)$ is falling fast there. In principle, this could lead to ambiguities in fitting the $\eta_2(2030)$, but we find that this state is produced in a different range of beam momenta, so in practise there is no problem.

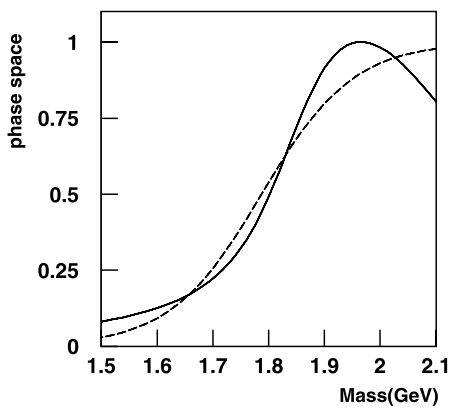

Fig. 3 $f_2(1270)\eta$ phase space (*full curve*) and an approximation with a Fermi function (*dashed*)

A further potential complication is that $(M^2 - s)$ of the Breit-Wigner denominator should strictly be replaced by $(M^2 - s - m(s))$ with

$$m(s) = \frac{s - M^2}{\pi} P \int \frac{M\Gamma_2 F(s')\, ds'}{(s' - s)(s' - M^2)}; \quad (16)$$

$m(s)$ is the 'running mass', which makes the formula fully analytic [17]. At a sharp threshold, $m(s)$ peaks strongly at the threshold. However, for a threshold as wide as $f_2\eta$, its effect is small and can be absorbed into optimised values of M and Γ_2.

In our earlier publication on the present data in the year 2000, a sizable $a_0(980)\sigma$ amplitude was fitted. It accounted for ~15% of the $\eta 3\pi^0$ cross section, see Fig. 2(a) of Ref. [3]. It was fitted using the 1993 parametrisation of the σ amplitude by Zou and Bugg [18]. Since then, the understanding of the σ amplitude has improved greatly through the work of Caprini et al. [19], using the Roy equations. That work fits the $\pi\pi$ scattering length to $(0.220 \pm 0.005)m_\pi^{-1}$ and alters the s-dependence of the $\pi\pi$ amplitude below 600 MeV quite significantly. In addition, there is now evidence for significant coupling of the σ to KK: $g^2_{KK}(\sigma)/g^2_{\pi\pi}(\sigma) = 0.6 \pm 0.15$ [20]. We now use Eqs. (1)–(11) of [21] for the σ; they fit accurately the predictions of Colangelo et al. up to 1 GeV and fit better the inelasticity required above the KK threshold. The additional structure in the $\pi\pi$ amplitude is modest, but enough that the evidence for the $a_0(980)\sigma$ amplitude in present data almost disappears. The remaining signal is barely a 2 standard deviation effect. It is now omitted and systematic errors covering the possible signal will be included in branching ratios discussed below in Sect. 4.2. The earlier $a_0(980)\sigma$ signal was perturbing the fit via interferences with $a_0(980)$ signals from decays of $\eta_2(1645)$, $\eta_2(1870)$ and $\eta_2(2030)$. A consequence is that there are now rather large changes to the branching ratios of the $\eta_2(1870)$ and $\eta_2(2030)$ to $a_0(980)\pi$. The basic difficulty here is that the earlier broad σ amplitude had little structure and gave a rather flexible fit to the data. The branching ratios of $\eta_2(1645)$ and $\eta_2(1870)$ to $f_2(1270)\eta$ and $a_2(1320)\pi$ are more robust and change little.

The $\sigma \to \pi\pi$ amplitude is needed only up to ~1100 MeV. Its form for elastic scattering is known quite precisely. In elastic scattering, it is parametrised in the form $N(s)/D(s)$, where the numerator contains an Adler zero just below threshold, making the amplitude weak at low momenta. In some production processes with large momentum transfers, e.g. $J/\Psi \to \omega\sigma$, the numerator needs to be replaced with a constant in order to reproduce a broad peak in the mass range 450–500 MeV, produced by a pole in $D(s)$. In the present data, there is no evidence for this behaviour, so the amplitude is taken to be that of elastic scattering.

3 Fits to data

In order to demonstrate the existence of $\eta_2(1645)$, $\eta_2(1870)$ and $\eta_2(2030)$, it is necessary to fit data at all beam momenta and show that various selections of events require the presence of all three, with consistent masses, widths and ratios of decay amplitudes at all beam momenta. The earliest publication studied data at just two beam momenta, 1200 and 1940 MeV/c [2]. It was immediately obvious that these two momenta required two resonances $\eta_2(1645)$ and $\eta_2(1870)$, produced with considerably different relative intensities at the two momenta. The $\eta_2(1870)$ has a strong decay to $f_2(1270)\eta$ and the $\eta_2(1645)$ does not. The picture developed further when data at all nine beam momenta were available. A further $\eta_2(2030)$ was required, with a distinctive decay to $[a_2\pi]_{L=2}$ [3]. Here we shall not repeat this lengthy story, but refer the reader to the original publications. The conclusion from all beam momenta combined is that just these three states are sufficient to fit all the data, with consistent decay amplitudes at all beam momenta. Here we simply illustrate the quality of fits to mass projections.

Figure 4 shows mass projections for 3π, $\pi\pi\eta$, $\pi\eta$ and $\pi\pi$ at a beam momentum of 1642 MeV/c. Points with errors are data; fits are shown as histograms. In (a), there is a high mass peak due to $\pi_2(1670)\eta$, $\pi_2 \to f_2(1270)\pi$. In remaining panels there are peaks due to $f_1(1285)$, $a_0(980)$ and $a_2(1320)$ and a shoulder due to $f_2(1270)$.

At this beam momentum, the $\pi\pi\eta$ mass spectrum does not distinguish $\eta_2(1645)$, $\eta_2(1870)$ and $\eta_2(2030)$ cleanly. It is necessary to select events in the mass range 1500–1750 MeV to study properties of $\eta_2(1645)$. Figures 5(a) and 5(b) show $\pi\eta$ and $\pi\pi$ mass spectra for this selection. Panels (c) and (d) show mass projections for the $\pi\pi\eta$ mass range 1775–1975 MeV, centred on $\eta_2(1870)$; Figs. 6(a) and 6(b) show projections for the $\pi\pi\eta$ mass range 2.0–2.25 GeV. Taken together with angular dependence in the data, these projections constrain fits to $\eta_2(1645)$, $\eta_2(1870)$ and $\eta_2(2030)$ and their individual decay modes.

In order to display more clearly the $\eta_2(1870)$, Figs. 6(c) and 6(d) shows mass projections which select $a_2(1320)$ and reject $f_2(1270)$ or vice versa. In (c), $a_2\pi$ events are selected with $M(\pi\eta)$ in the mass range 1318 ± 55 MeV; events with $\pi^0\pi^0$ in the mass range 1.0–1.455 GeV are rejected. In (d), $f_2(1270)$ is selected in the mass range 1.1–1.37 GeV and events containing $\pi\eta$ in the mass range 1.15–1.435 GeV are vetoed. The strong $f_2(1870)$ peak in $f_2(1270)\eta$ is clearly visible in Fig. 6(d). In Fig. 6(c), one sees the combined $\eta\pi\pi$ mass spectrum from $\eta_2(1645)$ and $\eta_2(1870) \to a_2\pi$. Similar cuts in data selection illustrate the presence of $\eta_2(2030) \to [a_2\pi]_{L=2}$. Fits to data are of similar quality at all beam momenta; further examples were shown in Ref. [2].

In order to achieve good fits to data, the eleven channels of Sect. 1 need to be sub-divided to include separate channels for (i) $\eta_2(1645) \to a_2\pi$ and $a_0\pi$, (ii) $\eta_2(1870) \to f_2(1270)\eta$, $a_2\pi$ and $a_0\pi$, (iii) $\eta_2(2030) \to [a_2\pi]_{L=2}$, $[a_2\pi]_{L=0}$, $a_0\pi$ and $f_2(1270)\eta$, (iv) $f_2(1910) \to [a_2\pi]_{L=1}$ and $[f_2(1270)\eta]_{L=1}$, (v) $f_2(2001) \to [a_2\pi]_{L=3}$ only, (vi) $f_2(2240) \to [a_2\pi]_{L=1,3}$ and $[f_2(1270)\pi]_{L=1,3}$. At each beam momentum, phases for all these channels are fitted freely.

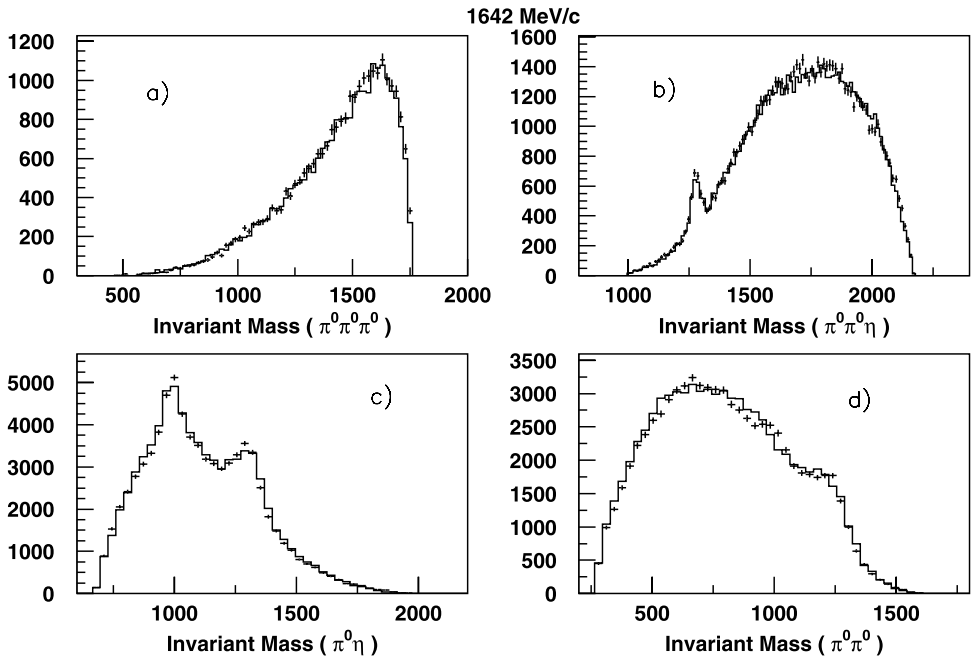

Fig. 4 Mass spectra for (**a**) 3π, (**b**) $\eta\pi\pi$, (**c**) $\eta\pi$ and (**d**) $\pi\pi$ at a beam momentum of 1642 MeV/c. Histograms show fits to data

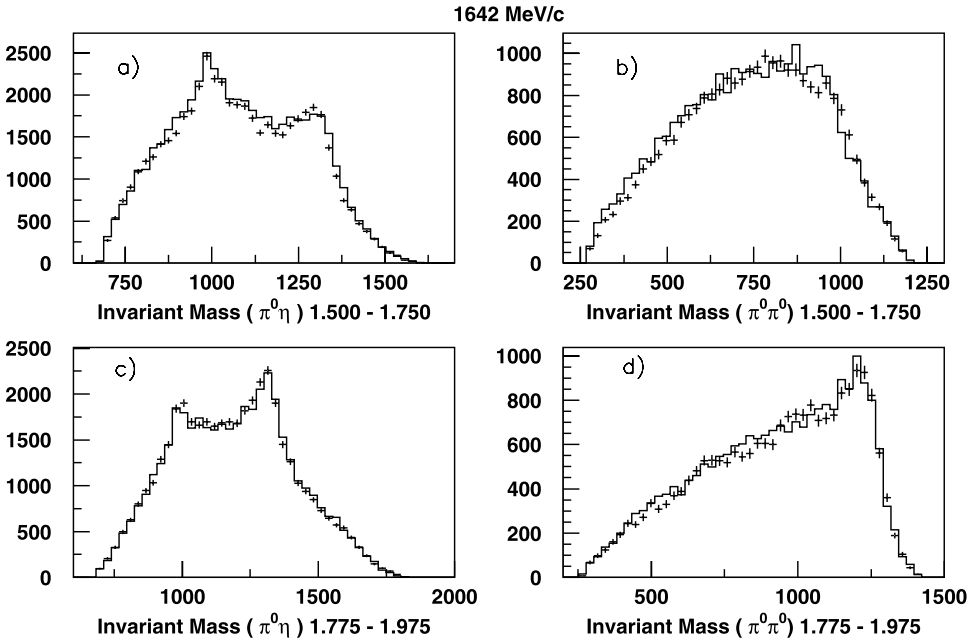

Fig. 5 Mass spectra at 1642 MeV/c for (**a**) and (**c**) $\pi^0\eta$ in two ranges of $M(\pi\pi\eta)$; (**b**) and (**d**) $\pi^0\pi^0$. Histograms show fits to data

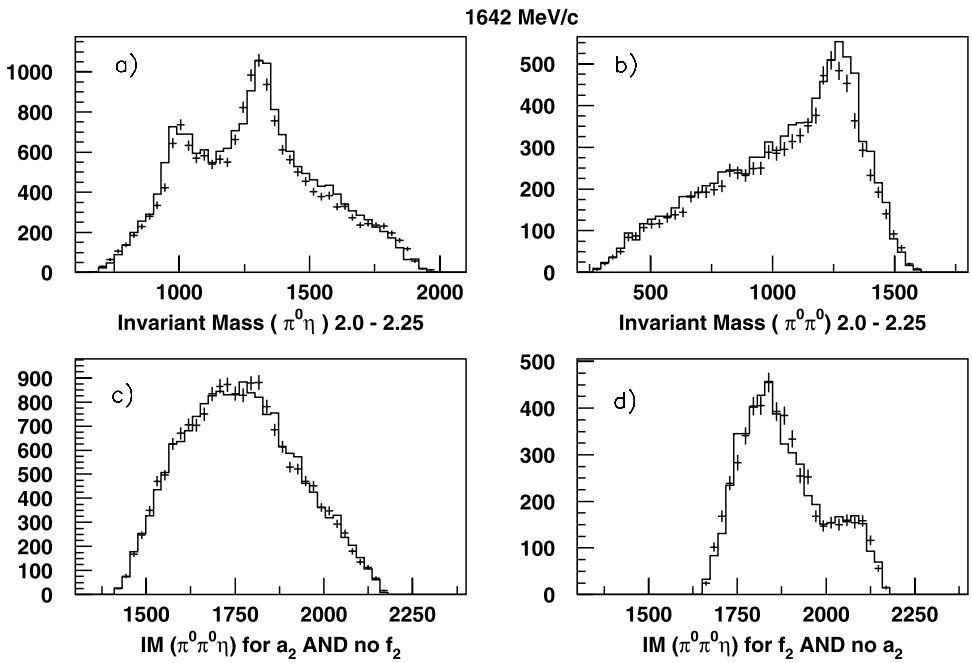

Fig. 6 Mass spectra at 1642 MeV/c for (**a**) and (**b**) $\pi^0\eta$ and $\pi^0\pi^0$ in the $M(\pi\pi\eta)$ mass range 2.0–2.25 GeV; (**c**) the $\pi\pi\eta$ mass spectrum selecting a_2 and vetoing $f_2(1270)$; (**d**) the converse selection. Histograms show fits to data

In earlier work, there was some evidence for $\eta_2(1870) \to [\eta\sigma]_{L=2}$. There remains a small improvement in log likelihood when this channel is included. This improvement is however typically 30, which is less than for almost all other channels. Furthermore, its inclusion increases errors on other channels, i.e. fits become less stable including it. The problem is that there is no narrow signature of the $\sigma \to \pi\pi$ S-wave, so it tends to absorb any noise in the data. This decay is now omitted.

4 Results

Table 1 shows changes in log likelihood when each channel is omitted from the fit and all other channels are re-optimised. One sees immediately the significance level of each channel and its dependence on beam momentum.

We now wish to draw conclusions from peaks observed in some channels of data. Figure 7 shows cross sections vs. beam momentum. The absolute normalisation is taken from

Table 1 Changes in log likelihood when each channel is removed from the fit and others are re-optimised

Momentum (MeV/c)	1050	1200	1350	1525	1642	1800	1940
Events	15709	35127	26379	21339	25394	28200	31388
Channel							
f_2a_0	163	344	408	471	409	357	281
$a_2\sigma$	195	353	455	268	316	179	249
$\pi_2(1670)\pi$	–	337	384	381	655	790	390
$\eta_2(1645) \to a_2\pi$	98	162	240	226	367	295	445
$\eta_2(1645) \to a_0\pi$	8	19	97	57	100	52	44
$\eta_2(1870) \to f_2\eta$	206	227	169	134	149	285	324
$\eta_2(1870) \to a_2\pi$	39	127	66	35	57	21	80
$\eta_2(1870) \to a_0\pi$	26	35	23	25	9	12	23
$\eta_2(2030) \to [a_2\pi]_{L=2}$	161	294	336	367	440	438	203
$\eta_2(2030) \to [a_2\pi]_{L=0}$	9	17	21	6	9	12	1
$\eta_2(2030) \to f_2\eta$	42	101	150	124	109	111	39
$\eta_2(2030) \to a_0\pi$	77	88	45	55	90	14	14
$f_2(1910) \to [a_2\pi]_{L=1}$	359	644	330	223	269	179	96
$f_2(1910) \to [f_2\eta]_{L=1}$	17	27	37	49	112	54	71
$f_2(2001) \to [a_2\pi]_{L=3}$	22	20	63	152	279	88	27
$f_2(2240) \to [a_2\pi]_{L=1,3}$	–	–	–	–	–	432	995
$f_2(2240) \to [f_2\eta]_{L=1,3}$	–	–	–	–	–	19	28

cross sections determined in Ref. [3] for the whole $\eta 3\pi^0$ data; they are uncorrected for branching fractions of η and $\pi^0 \to \gamma\gamma$ and therefore correspond directly to the number of events collected. The integrated cross section varies little with beam momentum, with a small (10%) enhancement near 2270 MeV; it is shown in Fig. 2 of Ref. [3]. In Fig. 7, smooth curves for individual channels (2)–(12) are drawn through the data within one standard deviation. Errors are typically 5–10% and some examples will be displayed with errors in Fig. 8. Cross sections for several channels expand at low beam momenta 900 and 600 MeV/c to follow the $1/v$ dependence of the total cross section, where v is the beam velocity in the centre of mass.

In Fig. 7(b), there is a strong peak in the channel f_2a_0 near 2250 MeV and a broader peak in $\eta_2(2030)\pi$ at slightly higher mass. There is a possible peak in $\eta_2(1645)\pi$ in the same mass range. There is also a peak in $f_2(1910)\pi$ near 2150 MeV. The channel $\pi_2(1670)\eta$ peaks strongly at high mass. There is evidence for production of $f_2(2240)\pi$ at the highest two beam momenta. Other channels show only weak structure, except that $a_2\sigma$ peaks at low masses.

The question arises how to interpret the peaks. Are they due to resonances? Here it is necessary to take care over details in the formulae. The amplitude for a resonance such as $a_2(2255) \to f_2(1270)a_0$ is

$$A = \sqrt{\rho(\bar{p}p, s)\rho(f_2a_0, s)}/\big[k\big(M^2 - s - iM\Gamma_{\rm tot}\big)\big]. \qquad (17)$$

The factor k in the denominator is the momentum of the $\bar{p}$ in the $\bar{p}p$ centre of mass; this is the flux factor for the incident beam. The phase space factor for $\rho(\bar{p}p, s)$ in the numerator is $k/\sqrt{s}$, multiplied by a centrifugal barrier factor. We choose to make comparisons with data by accounting explicitly for the intensity factors $k/\sqrt{s}$ for $\bar{p}p$ and $1/k^2$ from the flux factor; the two together give a factor $1/k\sqrt{s} = 1/v$, where v is relativistic velocity. We multiply cross sections of Fig. 7 by a factor v/v_0, where v_0 is evaluated at 2410 MeV, the highest data point. Remaining centrifugal barrier factors and form factors are less certain and are modelled in the fit to results.

Figure 8 shows data for $(v/v_0)\sigma$. For f_2a_0 in Fig. 8(a), there is a peak closely resembling the $a_2(2255)$, reported in the earlier combined analysis of $I = 1$, $C = +1$ CBAR data with $M = 2255 \pm 20$ MeV and $\Gamma = 230 \pm 15$ MeV; it was observed as a clear peak in data for $\bar{p}p \to f_2(1270)\pi$, see panel ($\ell$) of Fig. 38 of Ref. [5]. It was observed in both ${}^3F_2$ and ${}^3P_2$ decays to $f_2(1270)\pi$, with an amplitude ratio -2.13 ± 0.20 favouring coupling of $\bar{p}p$ to ${}^3F_2$. The dashed curve of Fig. 8(a) shows the remaining phase space factor calculated with this ratio for ${}^3F_2$ and ${}^3P_2$ production and with S-wave decay to f_2a_0. The rise of this curve with mass fails to fit the data. Any other ratio of ${}^3P_2$ and ${}^3F_2$ also fails to fit the data. Adding P-state f_2a_0 decays makes the dashed curve peak even higher in mass.

The full curve shows the result of multiplying the dashed curve by the line-shape of $a_2(2255)$, assuming a Breit-

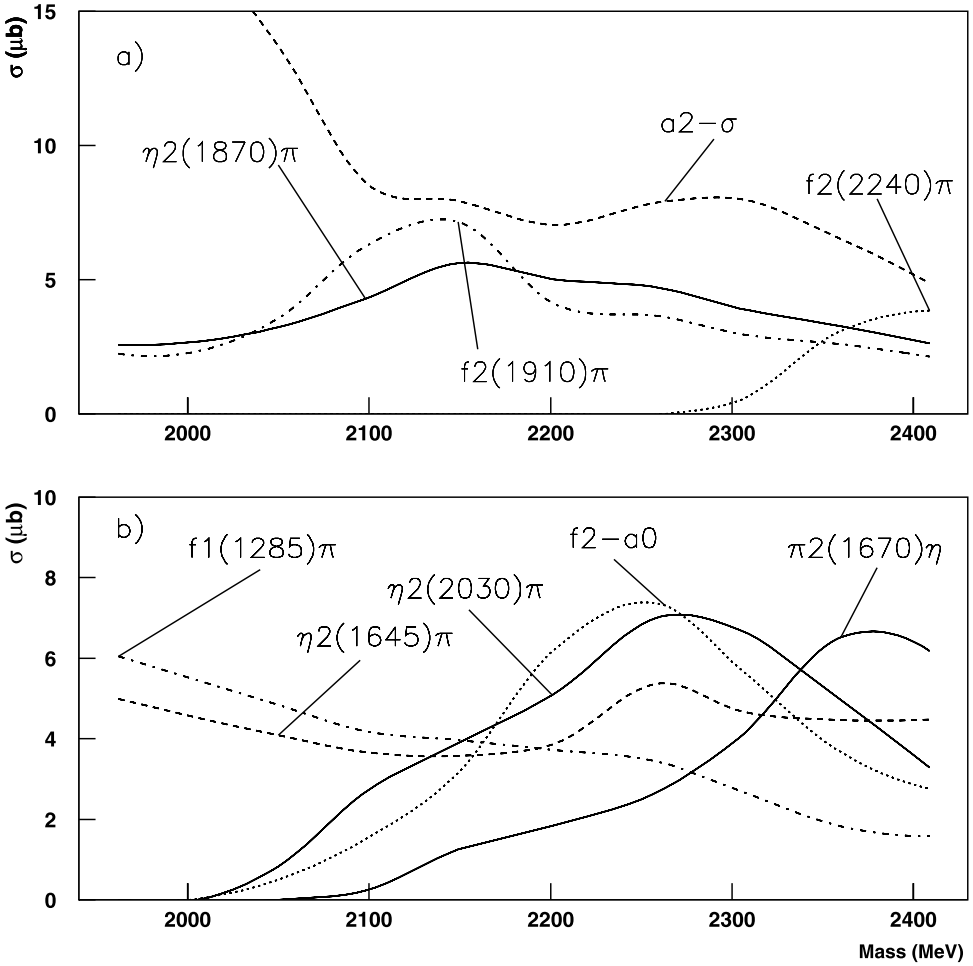

Fig. 7 Cross sections for each final state. Smooth curves are drawn through cross sections for each channel

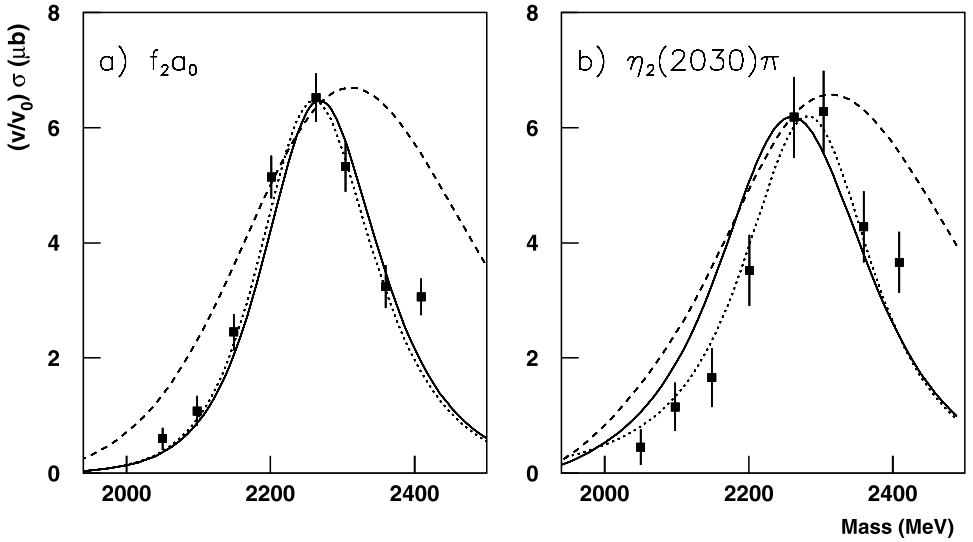

Fig. 8 Production of (**a**) $f_2(1270)a_0$ compared to phase space for S-wave production (*dashed curve*), a fit to $f_2(2255)$ (*full curve*) and a fit with parameters of this state optimised (*dotted curve*); (**b**) $\eta_2(2030)\pi$ compared to phase space for P-state production (*dashed curve*), a fit using the line-shape of $\pi_2(2245)$ (*full curve*) and a fit with parameters of this state optimised (*dotted*)

Wigner resonance of constant width. It is remarkably close to the data. We regard this as further confirmation of the $a_2(2255)$. A small improvement is possible by reducing the mass by 10 to 2245 MeV and decreasing the width to 225 MeV, but these changes are within the errors of the earlier determination and also within errors of present data.

Figure 8(b) shows results for the channel $\eta_2(2030)\pi$. Production of this final state is dominantly ($\sim 74\%$) with

$\bar{p}p$ helicity 0, suggesting production via $\bar{p}p \to \pi_2(2245)$:

$$\bar{p}p \to \pi_2(2245) \to [\eta_2(2030)\pi]_{\ell=1} \tag{18}$$

$$\eta_2(2030) \to [a_2\pi]_{L=2} \tag{19}$$

$$a_2(1320) \to [\eta\pi]_{L=2}. \tag{20}$$

The full amplitude D for this process is rather distinctive. Suppose it is written in fixed axes in the $\bar{p}p$ centre of mass. The initial state is spin singlet, helicity 0. Suppose the spectator pion of (18) is produced at angle θ of Fig. 2 and with azimuthal angle ϕ around the beam direction. Let the momentum of the decay pion in (18) be q. Let the decay angle of the $a_2(1320)$ in (20) after the Wick rotation be α, with azimuthal angle β, using the same axes as for (18). Then

$$D \propto \sqrt{\frac{1}{2}} q B_1(q) \sin\theta \sin\alpha \cos\alpha \left(e^{i(\phi-\beta)} - e^{-i(\phi-\beta)}\right) \tag{21}$$

$$= i\sqrt{2} q B_1(q) \sin\theta \sin\alpha \cos\alpha \sin(\phi-\beta). \tag{22}$$

Here $B_1(q)$ is the centrifugal barrier factor for $L = 1$ decay. The amplitude for the decay $a_2(2030) \to f_2(1270)\eta$ has an identical form. Amplitudes for decays of $a_2(2030) \to [a_0(980)\pi]_{L=2}$ take a similar form with angles α and β those of the decay pion. The amplitude for decays to $a_2(2030) \to [a_2(1320)\pi]_{L=2}$ involves a combination of spin 2 of the $a_2(1320)$ with $L = 2$ to make spin 2 of the $a_2(2030)$. This amplitude may be constructed along the same lines using Clebsch-Gordan coefficients or using tensor algebra. Because of the additional angular dependence on $L = 2$ in the decay to $[a_2(1320)\pi]_{L=2}$, it is particularly distinctive and stands out clearly in the data.

From earlier work, the parameters of $\pi_2(2245)$ have sizable errors, $M = 2245 \pm 60$ MeV, $\Gamma = 320^{+100}_{-40}$ MeV [11]. The full curve of Fig. 8(b) shows a fit with these parameters; the width is clearly too large and the mass somewhat too low.

Production of $\eta_2(2030)\pi$ is $(26 \pm 4)\%$ in intensity from $\bar{p}p$ helicity 1 at the peak; this helicity 1 component may be accommodated with $a_2(2255) \to$ S-wave $\eta_2(2030)\pi$. Note that $a_2(2255)$ cannot contribute to $[\eta_2(2030)\pi]_{\ell=1}$. Also $[\eta_2(2030)\pi]_{\ell=2}$ has a strong variation with mass and will be strongly suppressed by the $\ell = 2$ centrifugal barrier. The dotted curve of Fig. 8(b) is obtained by adjusting the mass and width of π_2 to $M = 2285 \pm 20(stat) \pm 25(syst)$ MeV, $\Gamma = 250 \pm 20(stat) \pm 25(syst)$ MeV and including 26% of the intensity via $a_2(2255)$.

The data determine relative phases of strong channels with errors of $\sim \pm 15°$ at every momentum. The phase variation of f_2a_0 and $a_2(2030)\pi$ channels agree within these errors. If f_2a_0 is resonant, then so is $a_2(2030)\pi$ and this can only be explained in terms of some combination of $\pi_2(2245)$ and $a_2(2255)$. There are further triplet states $a_3(2275)$ and $a_1(2245)$ in this vicinity, but they can only contribute to decays to $[\eta_2(2030)\pi]_{\ell=2}$; this is inconsistent with the observed line-shape of the peak and can only make a small contribution to the data. Systematic errors assigned to the mass and width of $\pi_2(2245)$ cover any weak contribution from this source.

4.1 Other channels

The production of $\eta_2(1875)\pi$ is distinctively different to that of $\eta_2(2030)\pi$. Production from the initial $\bar{p}p$ system with helicity ± 1 is strongly dominant, requiring an initial triplet state. However, no conclusion can be drawn from the slowly varying cross section in Fig. 7(a). A minor correction to Ref. [3] is that the $\eta_2(1875)\pi$ signal plotted there in Fig. 2(a) was multiplied by a factor 2 to make it clearly visible; the intensity recorded there is close to the present analysis.

Production of $f_2(1910)\pi$ is roughly equal from initial states with helicity 0 and 1, but shows significant slow variation with mass. This is possible from initial triplet states. The peak near 2150 MeV may indicate production from the initial state $a_2(2175)$.

Production of $\pi_2(1670)\eta$ is dominantly via $\bar{p}p$ helicity 1, (i.e. spin triplet) but again fluctuates smoothly with mass by more than a factor 2. No firm conclusion can be drawn from the variation of cross section with mass.

A final point is that data are available at 900 MeV/c and were included in the earlier analysis [3]. However, there are small cross sections for several channels and these are difficult to determine with confidence. This beam momentum has been studied, but is discarded from the present analysis because of substantial systematic errors in weak channels. There are also low statistics at 600 MeV/c, and this momentum is omitted for the same reason.

4.2 Branching fractions

Fortunately, the branching fractions of $\eta_2(1645)$, $\eta_2(1870)$ and $\eta_2(2030)$ are not sensitive to the question whether or not their production goes directly via resonances in the $\bar{p}p$ channel. If such resonances are involved, all decay modes of these channels pick up the same phase variation from the production process. The dominant decay of $\eta_2(2030)$ is to $[a_2\pi]_{L=2}$; that for $\eta_2(1870)$ is to $f_2(1270)\eta$ and that for $\eta_2(1645)$ is to $a_2\pi$. Branching fractions will be quoted with respect to these dominant channels. Some of the smaller branching fractions have changed significantly since the analysis of the year 2000.

A general comment is that data determine ratios of amplitudes rather than ratios of intensities. That is, log likelihood has a parabolic minimum as a function of the amplitude ratio. The procedure is therefore to fit data using, for example, the magnitude of the $\eta_2(1645) \to a_2\pi$ amplitude as one variable and the ratio of amplitudes $\eta_2(1645) \to$

Table 2 Variation of acceptance (including form factors) with beam momentum

Momentum (MeV/c):		1050	1200	1350	1525	1642	1800	1940
Resonance	Ratio							
$\eta_2(1645)$	$a_0\pi/a_2\pi$	0.955	0.974	0.986	0.990	0.993	0.997	1.0
$\eta_2(1870)$	$a_2\pi/f_2\eta$	2.32	1.80	1.50	1.31	1.13	1.06	1.0
	$a_0\pi/f_2\eta$	2.01	1.51	1.13	1.04	1.01	1.001	1.0
$\eta_2(2030)$	$[a_2\pi]_{L=0}/[a_2\pi]_{L=2}$	1.78	1.57	1.34	1.19	1.08	1.04	1.0
	$a_0\pi/[a_2\pi]_{L=2}$	1.57	1.43	1.26	1.15	1.09	1.04	1.0
	$f_2\eta/[a_2\pi]_{L=2}$	0.98	1.00	1.01	1.02	1.01	1.01	1.0
$f_2(1910)$	$f_2\eta/a_2\pi$	0.738	0.803	0.871	0.917	0.948	0.976	1.0

Table 3 Branching ratios; column 4 shows values for present data and column 5 shows values corrected for all charges and all decay modes of f_2, a_2 and a_0

Resonance	Ratio	Ref. [3]	Present data	Corrected
$\eta_2(1645)$	$BR(a_0\pi)/BR(a_2\pi)$	0.36 ± 0.12	0.38 ± 0.13	0.074 ± 0.025
$\eta_2(1870)$	$BR(a_2\pi)/BR(f_2\eta)$	0.22 ± 0.03	0.28 ± 0.07	1.60 ± 0.40
$\eta_2(1870)$	$BR(a_0\pi)/BR(f_2\eta)$	0.85 ± 0.05	0.48 ± 0.45	0.48 ± 0.45
$\eta_2(2030)$	$BR(a_0\pi)/BR([a_2\pi]_{L=2})$	0.37 ± 0.08	0.59 ± 0.50	0.10 ± 0.08
$\eta_2(2030)$	$BR(f_2\eta)/BR([a_2\pi]_{L=2})$	0.43 ± 0.15	0.75 ± 0.34	0.13 ± 0.06
$\eta_2(2030)$	$BR[a_2\pi]_{L=0}/BR([a_2\pi]_{L=2})$	–	0.05 ± 0.03	0.05 ± 0.03
$f_2(1910)$	$BR(f_2\eta)/BR(a_2\pi)$	–	0.54 ± 0.29	0.09 ± 0.05

$a_0\pi/\eta_2(1645) \to a_2\pi$ as the second. This makes it easy to investigate fluctuations with beam momentum. The average of each ratio of amplitudes is found by weighting values at each beam momentum with the total number of $a_2(1645)$ events summed over both channels. The same procedure is used for $\eta_2(1870)$, $\eta_2(2030)$ and $f_2\pi$ channels like $f_2(1910)\pi$. This gives more stable results than trying to determine errors of ratios at each momentum and using them in the weighting procedure; errors fluctuate somewhat from momentum to momentum because of large errors for phases fitted to weak channels. Having found the average ratios of amplitudes, a second pass is made through the fit, fixing these ratios at all momenta. Then the ratio of intensities is obtained from the total number of events fitted to each channel, integrated over all beam momenta.

In evaluating branching ratios, it is necessary to make use of (13)–(15). Here there is a dilemma. It is convenient to parametrise the Breit-Wigner denominator as far as possible with constant widths for each decay channel, as is conventional in the Particle Data Tables. Our procedure is to modify the numerator of (15) to $\Gamma_2 F(s)$, so as to agree with the denominator. We then evaluate branching ratios at each beam momentum, and average over momenta to determine Γ_1/Γ_2. This procedure converges within errors after one iteration. The same procedure is used to evaluate the effects of $L = 2$ centrifugal barriers on widths for $\eta_2(2030) \to [a_2\pi]_L = 2$ and $\eta_2(2030) \to [a_0\pi]_{L=2}$.

The acceptance for strong channels $f_2(1270)\eta$ and $[a_2\pi]_{L=2}$ varies rather strongly with beam momentum. Numerical results are shown in Table 2, normalised to 1 at the highest beam momentum 1940 MeV/c; they are evaluated using the Monte Carlo simulation of the detector. One sees a large variation of the intensity ratio R for some channels. This variation almost disappears at 1940 MeV/c, where all decay channels are nearly fully open. We shall tabulate branching ratios R corrected to this momentum. Above this momentum, results may be affected by errors in the Fermi function adopted in (14), so this is close to the optimum compromise. Errors in branching ratios due to these uncertainties are included in errors quoted in Table 3. We regard this procedure as an improvement on the work of Ref. [3], where branching ratios were evaluated purely from geometric acceptance without the effects of centrifugal barriers or the form factor $FF(s)$ of (13).

Coming to technicalities, it will be necessary to correct the number of observed $a_2(1320)\pi$ and $f_2(1270)\eta$ events in $\pi^0\pi^0\eta$ for unobserved decays. The $f_2(1270)$ has a branching ratio of 0.848/3 to $\pi^0\pi^0$ [10]. The amplitude for the $I = 1$ component of $\bar{p}p \to \pi X$, $X \to f_2\eta$ is given by

$$A(I=1) = \pi_1^0 X_{23}^0 + \pi_2^0 X_{31}^0 + \pi_3^0 X_{32}^0 \tag{23}$$

$$\to \sqrt{1/3}\big[\pi_1^0(\pi_2^0\pi_3^0)\eta + \pi_2^0(\pi_3^0\pi_1^0)\eta + \pi_3^0(\pi_1^0\pi_2^0)\eta\big]. \tag{24}$$

In (23), X stands for the amplitude of $X \to f_2\eta$; the brackets in the last line identify pions coming from $f_2(1270)$. For $X \to a_2\pi$, the decay amplitude of X is $\sqrt{1/3}(\pi^+ a_2^- - \pi^0 a_2^0 + \pi^- a_2^+)$, where the minus sign for $\pi^0 a_2^0$ can be absorbed into the fitted phase for this channel. In the $\pi^0 a_2^0$ final state, what is actually observed is

$$\begin{aligned} B(I=1) = \sqrt{1/6}\big(&\pi_1^0\big[\big(\pi_2^0\eta\big)\pi_3^0 + \big(\pi_3^0\eta\big)\pi_2^0\big] \\ &+ \pi_2^0\big[\big(\pi_3^0\eta\big)\pi_1^0 + \big(\pi_1^0\eta\big)\pi_3^0\big] \\ &+ \pi_1^0\big[\big(\pi_2^0\eta\big)\pi_3^0 + \big(\pi_3^0\eta\big)\pi_2^0\big]\big), \end{aligned} \tag{25}$$

i.e. six combinations. The coherent sum of all combinations is fitted to the data.

Table 3 shows in column 3 branching fractions from the previous analysis [3] for comparison purposes. The next column lists what is fitted now. The final column corrects this for all charge states and for the branching fractions of $a_2(1320) \to \pi\eta$ (14.5%) and $a_0(980)\pi$ to $\pi\eta$. This last branching fraction is taken to be the value used by WA102, (86%) for easy comparison with their results. This is close to the value adopted by the PDG [10]. If their value is adopted, $a_0(980)$ branching fractions increase by a factor 1.015 ± 0.021. Results in columns 4 and 5 supercede the earlier results.

Branching ratios of decays to $a_0(980)\pi$ final states are unstable. They depend somewhat on whether or not the $a_0(980)\sigma$ channel is included in the fit. The basic difficulty is that the σ amplitude is broad and gives rise to interferences all over the 4-body phase space. The $a_0\sigma$ channel is therefore not well determined. In the absence of definite evidence that it is needed, we omit it. All a_0 signals are weak and their phases with respect to dominant decays have quite large errors. There are also strong correlations between couplings of $\eta_2(1645)$, $\eta_2(1870)$ and $\eta_2(2030)$ to $a_0\pi$. In the earlier analysis, $a_0\pi$ decays interfered with $a_0\sigma$, giving apparently small but unreliable errors.

From the present analysis, the ratio for $\eta_2(1645)$ lies close to the WA102 result 0.077 ± 0.016; the $a_0(980)$ signal is clearly visible as a peak in their raw data [4]. For this reason, the weighted mean of these two values has been adopted and fixed for $\eta_2(1645)$. This helps stabilise fits to $a_0\pi$. However, there are large correlations between $\eta_2(1870)$ and $\eta_2(2030)$ decays to $a_0(980)\pi$. Together with uncertainties due to possible contributions from $a_0(980)\sigma$, the result is that branching fractions of $\eta_2(1870) \to a_0\pi$ and $\eta_2(2030)\pi$ can both vary freely over the range 0.1 to 0.85 in present data. Errors on values given in Ref. [3] for these two channels need to be increased substantially to take account of these systematic errors. New estimates are given in Table 3. These uncertainties are not significantly correlated with branching fractions to $f_2(1270)\eta$ and $a_2\pi$. Branching ratios between $f_2(1270)\eta$ and $a_2(1320)\pi$ decay modes are mostly quite stable, because these decays are strong. The ratio of decays of $\eta_2(1870)$ to $f_2(1270)\eta$ and $a_2(1320)\pi$ remains stable. So does the ratio of decays of $\eta_2(2030)$ to $f_2(1270)\eta$ and $[a_2\pi]_{L=2}$, because these are conspicuous decays.

A mistake has been located in the branching fraction of $\eta_2(2030)$ to $[a_2\pi]_{L=0}$ reported in Ref. [3]. The corrected value is given in entry 6 of Table 3. This decay is much weaker than that to $[a_2\pi]_{L=2}$.

Table 4 gives the important branching ratio of amplitudes $\eta_2(1870) \to a_2(1320)\pi / \eta_2(1870) \to f_2(1270)\eta$ at all beam momenta, in order to illustrate the stability. We choose to take the simple mean 0.298 over beam momenta, so as to avoid bias from fortuitous fluctuations in errors with beam momentum. Fluctuations about the mean are above statistics by a factor 1.4. The statistical error is increased to allow for this in Table 3.

In earlier work, the error on the mean was taken as the statistical error divided by $\sqrt{N}$, where N is the number of beam momenta. However, it is now clear that systematic errors are somewhat larger than this. The systematic errors are estimated from (i) variation of results with the ingredients included in the fit, particularly the number of interferences included between channels; (ii) variations with masses and widths of $\eta_2(1645)$, $\eta_2(1870)$, $\eta_2(2030)$, $f_2(1910)$, $f_2(2001)$ and $f_2(2240)$, (iii) possible contribution from $f_2(2293)$, (iv) uncertainties in the background from other final states. Ultimately, systematic errors dominate for all branching ratios, particularly for decays to the weak $a_0\pi$ channels.

Table 4 The ratio of amplitudes $\eta_2(1870) \to a_2(1320)\pi / \eta_2(1870) \to f_2(1270)\eta$ at individual beam momenta

Beam momentum (MeV/c)	Amplitude ratio $\eta_2(1870) \to a_2\pi / \eta_2(1870) \to f_2\eta$
1050	0.383 ± 0.067
1200	0.321 ± 0.034
1350	0.219 ± 0.050
1525	0.202 ± 0.058
1642	0.320 ± 0.050
1800	0.334 ± 0.063
1940	0.308 ± 0.065

5 Fits to WA102 data

The WA102 collaboration measured central production of $\pi\pi\eta$ and produced separate sets of data for $\eta \to \gamma\gamma$ and $\pi^+\pi^-\pi^0$ [4]. These data have been read from their graphs and refitted.

Their approach was to use the K-matrix for $\eta_2(1645)$ and $\eta_2(1870)$. If a single amplitude is used in this approach, the amplitudes for $\eta_2(1645)$ and $\eta_2(1870)$ each loop round the Argand circle once; continuity of the amplitude then requires a zero between them. The dip due to this zero played a significant part in fitting the data.

The basic assumption of the K-matrix approach is that resonances combine in a production process in an identical way to elastic scattering. This is a pure assumption. In elastic scattering, ingoing and outgoing waves for all coupled channels must sum asymptotically to unit intensity. However, in production processes considered here, the amplitude is only a tiny fraction of the $\bar{p}p$ total cross section. There is no obvious reason why 2-body unitarity should apply in the same way as for elastic scattering. The K-matrix approach has been tested on four sets of experimental data in Ref. [22]; it failed seriously in every case. If it is used, phases of $\eta_2(1645)$ and $\eta_2(1870)$ need to be fitted freely, since final states may rescatter between one another, generating phases which need to be fitted arbitrarily. Our analysis therefore uses the isobar model. This makes no assumption about the effects of unitarity and allows separate phases for $\eta_2(1645)$ and $\eta_2(1870)$.

Refitted results are displayed in Fig. 9. Data for $\eta \to \gamma\gamma$ and $\eta \to \pi^+\pi^-\pi^0$ have been fitted simultaneously, including decays to all of $a_0(980)\pi$, $f_2(1870)\eta$ and $a_2(1320)\pi$. They have been fitted with and without $\eta_2(2030)$. That component was not known at the time of the WA102 analysis. Full curves in Fig. 9 show fits without $\eta_2(2030)$ and dashed curves the fits including it. With it, the total χ^2 improves from 124.5 to 95.8. The reason is obvious: it provides extra freedom in fitting small defects in the mass region above 2 GeV. This improvement in χ^2 of 28.7 needs to be balanced against the fact that there are three extra complex coupling constants for the three channels of $\eta_2(2030)$, i.e. 6 extra fitting parameters. The improvement in χ^2 is 3.6 standard deviations. It is debatable whether or not $\eta_2(2030)$ is really present. Conclusions will be drawn here from fits without it; these fits are more secure.

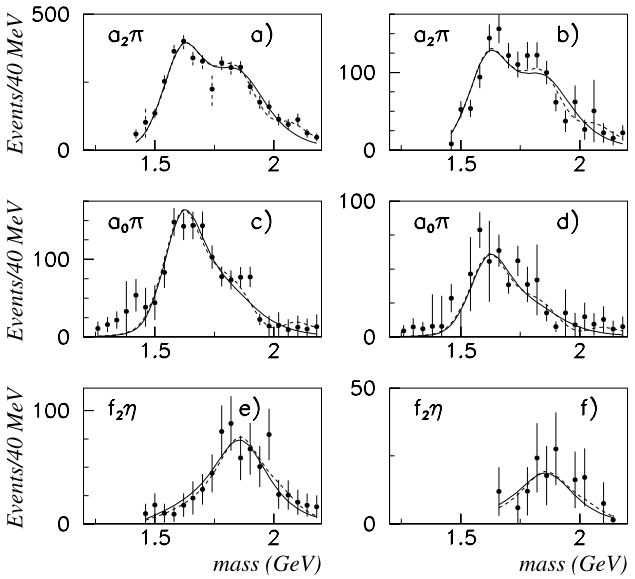

Fig. 9 Fits to WA102 data for central production of $a_2\pi$, $a_0\pi$ and $f_2(1270)\eta$ with $J^{PC} = 2^{-+}$. The *first column* shows data for $\eta \to \gamma\gamma$ and the *second* data for $\eta \to \pi^+\pi^-\pi^0$. *Full curves* are fits without $\eta_2(2030)$ and *dashed curves* with it

A significant point is that the K-matrix zero between the 1645 and 1870 MeV peaks made both of them narrower and pushed the peaks apart. In the WA102 fit, the mass of $\eta_2(1645)$ was 1605 ± 12 MeV for $\eta \to \gamma\gamma$ data and 1619 ± 11 MeV for $\eta \to 3\pi$. These are to be compared with the CBAR determination of $1645 \pm 6(stat) \pm 20(syst)$ MeV. In the isobar model, the dip between the two resonances can be filled in by interferences between them. Table 5 shows fitted masses and widths for $\eta_2(1645)$ and $\eta_2(1870)$ for two cases. In the first, column 2, the parameters of $\eta_2(1870)$ are fitted freely.

The width of the $\eta_2(1870)$ tends to run away to a large value. In Fig. 9(d), the width of the $\eta_2(1870)$ peak in decays to $f_2(1270)\eta$ is sensitive to scatter in the points near the peak. The second fit (column 3) is made adding to χ^2 a contribution given by the CBAR masses and widths with statistical and systematic errors combined in quadrature. This extra constraint stabilises the fit and gives mass and width for $\eta_2(1870)$ closer to the CBAR values. In our opinion, the third column is the more reliable, bearing in mind that the addition of the $\eta_2(2030)$ increases the uncertainties from WA102 data even further.

The explicit re-arrangement of (15) for $\eta_2(1870) \to f_2(1270)\eta$ is

$$f = \frac{[0.685F(s)M\Gamma]^{1/2}}{[M^2 - s - i(0.672 + 0.685F(s))M\Gamma]}, \tag{26}$$

where M and Γ refer to values for $\eta_2(1870)$ in the last two lines of Table 6; $F(s)$ is given by (14). The CBAR data are fitted using (14) and (26). Numerical values in the denominator are such that $|f|^2$ integrated over s reproduces the branching fractions for $a_2\pi$, $a_0\pi$ and $f_2(1270)\eta$ in Table 3.

The line-shape of $\eta_2(1870)$ is shown in Fig. 10 and is very close to that of a Breit-Wigner resonance of constant width. It peaks at 1792 MeV. This is related to the opening of the $f_2(1270)\eta$ threshold. The pole position is at $1798 \pm 20 - i(130 \pm 12)$ MeV. If CBAR values are used instead, the imaginary part of the pole position decreases to 109 MeV.

Table 5 Masses and widths fitted to WA102 data without any constraint (column 2) and with a penalty function given by errors on CBAR masses and widths (column 3); Column 4 shows CBAR values of masses and widths

	Unconstrained fit	With CBAR constraint	CBAR values
χ^2	116.8	124.5	
$M(1645)$	1635 ± 12	1630 ± 9	$1645 \pm 6(stat) \pm 20(syst)$
$\Gamma(1645)$	252 ± 36	225 ± 16	$200 \pm 5(stat) \pm 25(syst)$
$M(1870)$	1833 ± 20	1829 ± 12	$1825 \pm 5(stat) \pm 15(syst)$
$\Gamma(1870)$	332 ± 45	293 ± 24	$221 \pm 20(stat)^{+50}_{-35}(syst)$

Table 6 Changes in log likelihood when the amplitudes for $\eta_2(1870)$ (i) are replaced by their modulus (no phase variation), (ii) use a denominator $A - m(s) - iM\Gamma(s)$, see text

Momentum (MeV/c)	(i)	(ii)
1050	43	31
1200	81	98
1350	106	120
1525	91	47
1642	95	55
1800	195	127
1940	199	86

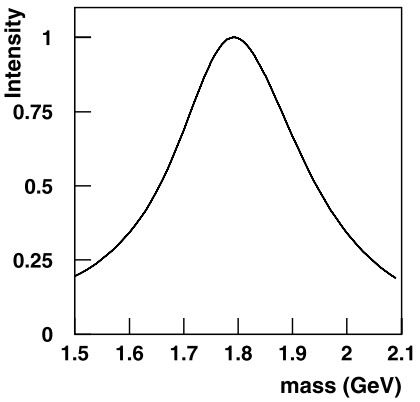

Fig. 10 The line-shape of $\eta_2(1870)$ from the combined fit to CBAR and WA102 data

The remaining question is whether there is really any significant $a_2(1320)$ signal in WA102 data due to $\eta_2(1870) \to a_2(1320)\pi$. In a 1997 publication [12], WA102 claimed to observe $\eta_2(1645) \to a_2(1320)\pi$ in central production of 4π, with a small shoulder at high mass which could be $\eta_2(1870)$. They reported a strong 2^+ signal in $a_2(1320)\pi \to \rho\pi\pi$ at 1900 MeV and a broad 2^+ peak in $f_2\pi\pi$ near 2000 MeV. The integrated 2^+ signal was considerably stronger than that for $J^P = 2^{-+}$. However, further data reported in the year 2000 on central production of 4π were interpreted in terms of $2^{-+} \to a_2(1320)\pi \to 4\pi$, produced only with $J_z = \pm 1$ [23]. The $2^{++} \to f_2(1270)\pi\pi$ was found again but no $2^{++} \to a_2(1320)\pi$. They make no comment on why this change from the 1997 work occurs. In

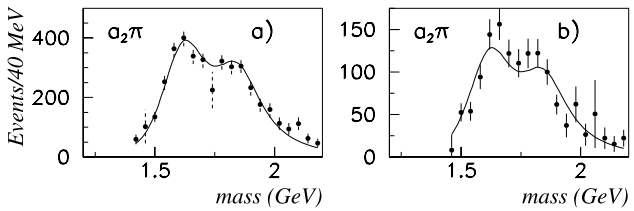

Fig. 11 Fits to WA102 data with $\eta_2(1870) \to a_2\pi$ replaced by $f_2(1910) \to a_2\pi$: (**a**) $\eta \to \gamma\gamma$, (**b**) $\eta \to \pi^+\pi^-\pi^0$

central production via Pomeron exchange, there is no obvious reason why 2^{++} should not be produced with $J_z = 0$, ± 1 and ± 2. Our view is that the data really need to be fitted with all allowed values of J_z for both $J^P = 2^+$ and 2^-. It would be valuable if the Compass collaboration could check this point.

In the CBAR data analysed here, there is clear evidence for $f_2(1910)$ and $f_2(2001)$ decaying to $a_2(1320)\pi$ and $f_2(1270)\eta$. The $a_2\pi$ decay dominates. This is readily understood from the fact that the $L = 1$ centrifugal barrier inhibits decay to $f_2(1270)\eta$. We suggest that the small bump claimed by WA102 in $a_2(1320)\pi$ at 1860 MeV is due to $f_2(1910)$. We have fitted WA102 data using PDG parameters $M = 1903$, $\Gamma = 196$ MeV for $f_2(1910)$ instead of $\eta_2(1870)$. The fit, shown in Fig. 11, gives a slightly improved description of the data (by 11 in χ^2), but we are unable to go back to the original data and check the J^P analysis.

It remains an interesting question why $\eta_2(1870)$ has a fairly large $f_2(1270)\eta$ S-wave decay. The dispersive term $m(s)$ of (17) leads to attraction in this channel near threshold [17]. It necessarily favours this decay mode. There is an isospin partner $\pi_2(1880)$ for $\eta_2(1870)$. It too has a strong decay mode to $a_2(1320)\eta$ [24].

6 Evidence that the $\eta_2(1870)$ is resonant

Several checks have been made that the $\eta_2(1870)$ has resonant phase variation. The first check is to remove the phase variation by replacing the amplitude by its modulus and refitting the data. At all beam momenta, this leads to a highly significant worsening of log likelihood. Column 2 of Table 5 shows the changes against beam momentum. The definition

of log likelihood is such that a change of 0.5 in log likelihood should correspond to a one standard deviation change. We have already remarked that fluctuations in Table 4 are a factor 1.4 above statistics. A more extensive examination of fluctuations in branching ratios shows they are in some cases up to a factor 2 above statistics, and that has already been taken into account in errors quoted in Table 3. Adopting this as a general rule leads to the conclusion that changes listed in Table 3 can be equated to changes in χ^2. They average to 11.6 standard deviations per momentum, i.e. 28σ in total.

The second check is that including the dispersive term of (16) into the Breit-Wigner denominator has little effect on log likelihood after minor alterations to fitted mass and width, well within errors quoted in Table 6. The dispersive term peaks at the $f_2(1270)\eta$ threshold, but with a large full width of ∼300 MeV. Numerically, it is easily absorbed into small shifts of fitted parameters.

There remains the possibility that the associated cusp in the real part of the amplitude could explain the phase variation without a resonance. The third check is to replace the Breit-Wigner denominator of (15) by

$$D = A - m(s) - iM\big[\Gamma_1 + \Gamma_2 F(s)\big]. \tag{27}$$

This removes the resonance by changing $M^2 - s$ to a constant A; it is the term in s which drives the real part of the amplitude through zero on resonance. Figure 12 shows the Argand diagram of the amplitude fitted to WA102 data. [The vertical scale is no longer limited to 1 at the peak, because the imaginary part of the amplitude no longer needs to reach 1 in the absence of a resonance.]

The imaginary part of the amplitude is forced by the data to peak at ∼1810 MeV, as before. The real part is positive everywhere. It turns out that the data do not force the constant A to go negative; instead it optimises close to +0.5. Then fits to $\eta 3\pi^0$ data are worse than for a resonance by the amounts shown in column 3 of Table 6. At the lowest three beam momenta, where the $\eta_2(1870)$ is strongest, results are similar to column 2. At higher momenta, the changes drop by roughly a factor 2. The reason for this drop has been traced to the fact that the phase variation in Fig. 12 adds a degree of freedom in the fit compared with column 2, where there is no phase variation at all. However, the significance levels in column 3 still average 9 standard deviations per momentum. If any phenomenologist wishes to develop a more complete dynamical model, the data are publicly available from the authors. Meanwhile, the evidence for resonant behaviour appears to be strong.

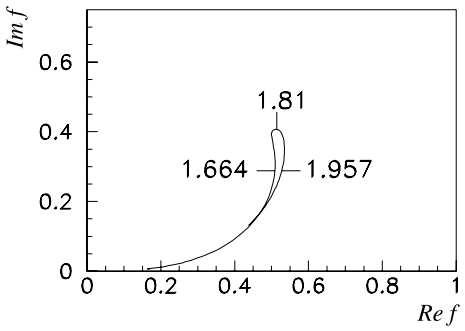

Fig. 12 The Argand diagram for a fit to WA102 data using (26)

7 Conclusions

This work confirms that the $\eta_2(1870)$ has a branching fraction to $f_2(1270)\eta$ comparable with that to $a_2(1320)\pi$, in agreement with our earlier analysis. It is not possible to fit these data with the large branching fraction found by WA102. Results of the two experiments agree well for the mass and width of $\eta_2(1645)$ and the branching fraction of its decays to $a_0(980)\eta$. They also agree quite well for the mass and width of $\eta_2(1870)$ from decays to $f_2(1270)\eta$. Small branching fractions reported in Table 2, particularly for decays to $a_0\pi$, have changed significantly from earlier values for a complex of reasons which are understood.

The WA102 collaboration has found evidence for a weak decay mode of $\eta_2(1645) \to K\bar{K}\pi$ [25] (7% of that for decays to $a_2\pi$); however, they find no evidence for $\eta_2(1870)$ in the same data. It therefore appears unlikely that the $\eta_2(1870)$ is the $s\bar{s}$ partner of $\eta_2(1645)$ and $\pi_2(1670)$. Figure 13 shows trajectories of $I = 0$, $C = +1$ for several sets of quantum numbers. In (b) $\eta_2(1645)$, $\eta_2(2030)$ and $\eta_2(2267)$ are consistent with the ${}^1D_2$ trajectory with the same slope as the others.

Hybrids with $J^{PC} = 2^{-+}$ are predicted around 1900 MeV by Isgur and Paton [26] and Godfrey and Isgur [27]. The interpretation given by many authors, including ourselves [3], is that $\eta_2(1870)$ and $\pi_2(1880)$ make a hybrid pair, somewhat higher in mass than the $\pi_1(1600)$ of the PDG, whose average mass is now 1662 MeV. It would be valuable to search for $s\bar{s}g$ partners in J/Ψ decays at BES 3. Page [28] predicts that hybrids will decay dominantly to ${}^3P\ \bar{q}q$ plus a pion, in agreement with the strongest observed decay modes $a_2\pi$ and $f_2\eta$ of $\eta_2(1870)$. Predictions for their branching ratio are subject to systematic errors from (i) the effect of the dispersive attraction from the $f_2\eta$ threshold and (ii) possible mixing of the hybrid with $q\bar{q}$ 1D and 2S states. The phase space alone for $a_2\pi$ is 1.184 ± 0.023 times that for $f_2\eta$ after integrating over the line-shape of $\eta_2(1870)$ and taking account of the form factor $\exp[-(4.5 \pm 1.0)q^2]$.

Li and Wang propose that the $\eta_2(1870)$ is the $n = 2\ q\bar{q}$ state and $\eta(2030)$ is the $n = 3$ state [29]. However, this would required a trajectory with twice the slope of other J^P.

Afonin [30] has presented an interesting scheme to accommodate known light mesons. Its general features are appealing. However, we question the way $J^{PC} = 2^{-+}$ states

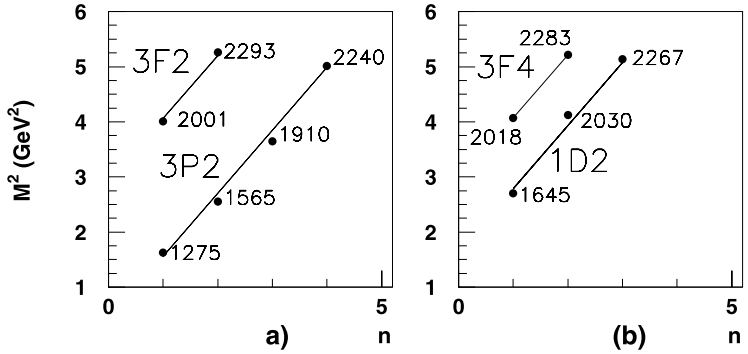

Fig. 13 Trajectories of resonances for several quantum numbers of $I = 0$, $C = +1$ states; masses are shown in MeV

Table 7 Changes in log likelihood when $\eta_2(2030)$ is removed from the fit to $\eta 3\pi^0$ data

Momentum (MeV/c)	Change in log likelihood
1200	408
1350	387
1525	420
1642	536
1800	484
1940	215

are included. He includes $\eta_2(1645)$, $\eta_2(1870)$ and $\eta_2(2250)$ for $I = 0$ and $\pi_2(1670)$, $\pi_2(2100)$ and $\pi_2(2245)$ for $I = 1$. The large mass difference between $\eta_2(1870)$ and $\pi_2(2100)$ is unexplained; the mass splitting between $\eta_2(1870)$ and $f_2(1934)$ is reversed for $\pi_2(2100)$ and $a_2(2030)$.

His model conflicts with present data, which require the presence of $\eta_2(2030)$; Table 7 shows changes in log likelihood if it is omitted and all other parameters are re-optimised. They are on average 1.18 × values in Table 7 for $\eta_2(2030) \to [a_2\pi]_{L=2}$, but they are not as large as the sum for all decays of $\eta_2(2030)$. This is because of correlations between decay channels. Nonetheless they are still highly significant. Furthermore, there is independent evidence for $\eta_2(2030)$ in $\bar{p}p \to \eta\pi\pi$ [6]. In those data, there is a strong peak with $M = 2040 \pm 40$ MeV, $\Gamma = 190 \pm 40$ MeV in $[f_2(1270)\eta]_{L=0}$ and a smaller, but still significant peak in $[f_2(1270)\eta]_{L=2}$; unfortunately the resonant phase variation cannot be checked in those data because there is no other strong feature in other singlet states near this mass.

The $\pi_2(1880)$ is listed by the PDG in four sets of data: (i) in $\eta\eta\pi$ with $M = 1880 \pm 20$ MeV by Anisovich et al. [31], (ii) in $\pi^- p \to \eta\pi^+\pi^-\pi^- p$ with $M = 2003 \pm 88 \pm 148$ MeV by E852 [32], (iii) in $\pi^- p \to \omega\pi^-\pi^0 p$ with $M = 1876 \pm 11 \pm 67$ MeV in further E852 data of Lu et al. [33], and (iv) in $\pi^- p \to \eta\eta\pi^- p$ with $M = 1929 \pm 24 \pm 18$ MeV by Eugenio et al. (E852) [24]. Of these, the second one could be $\pi_2(2005)$.

A further result from the present analysis is that there is evidence for the presence of $a_2(2255) \to f_2(1270)a_0(980)$ with parameters close to those of Ref. [11]. It is the third set of data in which it has been observed, the others being $\pi\eta$ and $3\pi^0$. There is also evidence that the channel $[\eta_2(2030)\pi]_{L=1}$ is produced via $\pi_2(2245)$; its mass and width are determined better by present data than by earlier analyses: $M = 2285 \pm 20(stat) \pm 25(syst)$ MeV, $\Gamma = 250 \pm 20(stat) \pm 25(syst)$ MeV. This is the third channel in which it has been observed.

Further data on $\eta 3\pi^0$ from a transversely polarised target would be very valuable. In such data, there are interferences between singlet and triplet states. It is likely that such information would allow a complete spin-parity analysis of the data, improving further on the present analysis.

Acknowledgements We thank the Crystal Barrel Collaboration for the use of the data.

Open Access This article is distributed under the terms of the Creative Commons Attribution Noncommercial License which permits any noncommercial use, distribution, and reproduction in any medium, provided the original author(s) and source are credited.

References

1. A.R. Cooper, Ph.D. thesis, University of London (1994)
2. J. Adomeit et al., Z. Phys. C **71**, 227 (1996)
3. A.V. Anisovich et al., Phys. Lett. B **477**, 19 (2000)
4. D. Barberis et al. (WA102 Collaboration), Phys. Lett. B **471**, 435 (2000)
5. D.V. Bugg, Phys. Rep. **397**, 257 (2004)
6. A.V. Anisovich et al., Nucl. Phys. A **651**, 253 (1999)
7. A.V. Anisovich et al., Phys. Lett. B **491**, 47 (2000)
8. E. Eisenhandler et al., Nucl. Phys. B **98**, 109 (1975)
9. A. Hasan et al., Nucl. Phys. B **378**, 3 (1992)
10. C. Amsler et al. (Particle Data Group), Phys. Lett. B **667**, 1 (2008)
11. A.V. Anisovich et al., Phys. Lett. B **571**, 261 (2001)
12. D. Barberis et al. (WA102 Collaboration), Phys. Lett. B **413**, 217 (1997)
13. A.V. Anisovich et al., Phys. Lett. B **472**, 168 (2000)
14. D.V. Bugg, Preprint arXiv:0907.3015 (2009)
15. C. Bourelly, E. Leader, J. Soffer, Phys. Rep. **59**, 95 (1980)
16. D.V. Bugg, A.V. Sarantsev, B.S. Zou, Nucl. Phys. B **80**, 59 (1996)
17. D.V. Bugg, J. Phys. G, Nucl. Part. Phys. **35**, 075005 (2008)
18. B.S. Zou, D.V. Bugg, Phys. Rev. D **48**, R3948 (1993)
19. I. Caprini, G. Colangelo, H. Leutwyler, Phys. Rev. Lett. **96**, 132001 (2006)

20. D.V. Bugg, Eur. Phys. J. C **47**, 45 (2006)
21. D.V. Bugg, J. Phys. G, Nucl. Part. Phys. **34**, 151 (2007)
22. D.V. Bugg, Eur. Phys. J. C **54**, 73 (2008)
23. D. Barberis et al. (WA102 Collaboration), Phys. Lett. B **471**, 440 (2000)
24. P. Eugenio et al., Phys. Lett. B **660**, 466 (2008)
25. D. Barberis et al. (WA102 Collaboration), Phys. Lett. B **413**, 225 (1997)
26. N. Isgur, J. Paton, Phys. Rev. D **31**, 2910 (1985)
27. S. Godfrey, N. Isgur, Phys. Rev. D **32**, 189 (1985)
28. P.R. Page, Phys. Lett. B **402**, 183 (1997)
29. D.-M. Li, E. Wang, Eur. Phys. J. C **32**, 297 (2009)
30. E. Afonin, Int. J. Mod. Phys. A **23**, 4205 (2009)
31. A.V. Anisovich et al., Phys. Lett. B **500**, 222 (2001)
32. J. Kuhn et al. (E852 Collaboration), Phys. Lett. B **595**, 109 (2004)
33. M. Lu et al. (E852 Collaboration), Phys. Rev. Lett. **94**, 032002 (2005)